9. P. N. Butcher, *J. Phys. Condens. Matter* **2**, 4869–4878 (1990).
10. C. L. Kane, M. P. A. Fisher, *Phys. Rev. Lett.* **76**, 3192–3195 (1996).
11. C. L. Kane, M. P. A. Fisher, *Phys. Rev. B* **55**, 15832–15837 (1997).
12. A. Greiner, L. Reggiani, T. Kuhn, L. Varani, *Phys. Rev. Lett.* **78**, 1114–1117 (1997).
13. L. G. C. Rego, G. Kirczenow, *Phys. Rev. B* **59**, 13080–13086 (1999).
14. I. V. Krive, E. R. Mucciolo, *Phys. Rev. B* **60**, 1429–1432 (1999).
15. M. P. Blencowe, V. Vitelli, *Phys. Rev. A* **62**, 052104 (2000).
16. D. R. Schmidt, R. J. Schoelkopf, A. N. Cleland, *Phys. Rev. Lett.* **93**, 045901 (2004).
17. C. Shannon, *Bell Syst. Tech. J.* **27**, 379–423 (1948).
18. K. Schwab, E. A. Henriksen, J. M. Worlock, M. L. Roukes, *Nature* **404**, 974–977 (2000).
19. C. S. Yung, D. R. Schmidt, A. N. Cleland, *Appl. Phys. Lett.* **81**, 31 (2002).
20. M. Meschke, W. Guichard, J. P. Pekola, *Nature* **444**, 187–190 (2006).
21. A. V. Timofeev, M. Helle, M. Meschke, M. Möttönen, J. P. Pekola, *Phys. Rev. Lett.* **102**, 200801 (2009).
22. L. W. Molenkamp, Th. Gravier, H. van Houten, O. J. A. Buijk, M. A. A. Mabesoone, C. T. Foxon, *Phys. Rev. Lett.* **68**, 3765–3768 (1992).
23. O. Chiatti *et al.*, *Phys. Rev. Lett.* **97**, 056601 (2006).
24. Y. X. Liang, Q. Dong, U. Gennser, A. Cavanna, Y. Jin, *J. Low Temp. Phys.* **167**, 632–637 (2012).
25. Materials and methods are available as supplementary materials on *Science* Online.
26. S. Jezouin *et al.*, *Nat. Commun.* **4**, 1802 (2013).
27. M. Büttiker, *Phys. Rev. Lett.* **65**, 2901–2904 (1990).
28. Y. M. Blanter, E. V. Sukhorukov, *Phys. Rev. Lett.* **84**, 1280–1283 (2000).
29. F. C. Wellstood, C. Urbina, J. Clarke, *Phys. Rev. B Condens. Matter* **49**, 5942–5955 (1994).
30. F. Pierre *et al.*, *Phys. Rev. B* **68**, 085413 (2003).
31. F. Giazotto, T. T. Heikkilä, A. Luukanen, A. M. Savin, J. P. Pekola, *Rev. Mod. Phys.* **78**, 217–274 (2006).
32. Y. Dubi, M. Di Ventra, *Rev. Mod. Phys.* **83**, 131–155 (2011).
33. F. Giazotto, M. J. Martínez-Pérez, *Nature* **492**, 401–405 (2012).

Acknowledgments: We gratefully acknowledge the contribution of V. Andreani to the noise measurement setup. This work was supported by the European Research Council (ERC-2010-StG-20091028, no. 259033).

Supplementary Materials

www.sciencemag.org/content/342/6158/601/suppl/DC1
Materials and Methods
Figs. S1 to S9
Table S1
References (*34*–*42*)

13 June 2013; accepted 16 September 2013
Published online 3 October 2013;
10.1126/science.1241912

Downloaded from www.sciencemag.org on January 1, 2015

Parameter Space Compression Underlies Emergent Theories and Predictive Models

Benjamin B. Machta,[1,2] Ricky Chachra,[1] Mark K. Transtrum,[1,3] James P. Sethna[1]*

The microscopically complicated real world exhibits behavior that often yields to simple yet quantitatively accurate descriptions. Predictions are possible despite large uncertainties in microscopic parameters, both in physics and in multiparameter models in other areas of science. We connect the two by analyzing parameter sensitivities in a prototypical continuum theory (diffusion) and at a self-similar critical point (the Ising model). We trace the emergence of an effective theory for long-scale observables to a compression of the parameter space quantified by the eigenvalues of the Fisher Information Matrix. A similar compression appears ubiquitously in models taken from diverse areas of science, suggesting that the parameter space structure underlying effective continuum and universal theories in physics also permits predictive modeling more generally.

Physics owes its success (*1*) in large part to the hierarchical character of scientific theories (*2*). These theories of our physical world model natural phenomena as if physics at macroscopic length scales were almost independent of the underlying, shorter-length–scale details. For example, understanding string theory or the electroweak interaction is not necessary for quantitatively modeling the behavior of solids or superconductors active on longer length and time scales. The fact that many lower-level theories in physics can be systematically coarsened (renormalized) into macroscopic effective models establishes and quantifies their hierarchical character.

A similar emergent simplicity also appears in other areas of science (*3*–*9*). In many cases, important predictions largely depend only on a few "stiff" combinations of parameters, followed by a sequence of geometrically less important "sloppy" ones (Fig. 1) (*10*–*12*). This recurring characteristic, termed "sloppiness," naturally arises (*13*, *14*) in models describing collective data (not chosen to probe individual system components) and has implications similar to those of the renormalization group (RG) and continuum limit methods of statistical physics. Both physics and sloppy models show weak dependence of macroscopic observables on microscopic details and allow effective descriptions with reduced dimensionality. To clarify this connection, we developed and applied an information theory–based generalization of sloppy model analysis to two well-understood physics models—a discrete model of diffusion and an Ising model of the ferromagnetic phase transition. For both models, we show that when observations are confined to long time or length scales, there is a similar compression of the microscopic parameter space, with sensitive or stiff directions corresponding to the relevant macroscopic parameters (such as the diffusion constant). These results suggest that the hierarchy of theories in physics relies on the same parameter space compression that is ubiquitous in general multiparameter models.

The sensitivity of model predictions to changes in parameters is quantified by the Fisher Information Matrix (FIM). The FIM forms a metric on parameter space that measures the distinguishability between a model with parameters θ^μ and a nearby model with parameters $\theta^\mu + \delta\theta^\mu$ (*15*–*18*). This divergence is given by $ds^2 = g_{\mu\nu}\delta\theta^\mu\delta\theta^\nu$, where $g_{\mu\nu}$ is the FIM defined by

$$g_{\mu\nu} = -\sum_{\vec{x}} P_\theta(\vec{x}) \frac{\partial^2 \log P_\theta(\vec{x})}{\partial\theta^\mu \partial\theta^\nu} \qquad (1)$$

Here, $P_\theta(\vec{x})$ is the probability that a (stochastic) model with parameters θ^μ would produce observables $\vec{x}$. In the context of nonlinear least squares, g is the Hessian of χ^2, the sum of squares of residuals of the data fit (*15*). Distance in this metric space is a fundamental measure of distinguishability in stochastic systems. Sorted by decreasing eigenvalues, eigenvectors of g describe progressively less important linear combinations of parameters that govern system behavior. Previously, it was shown that in nonlinear least squares models describing collective data, this metric's eigenvalues have logarithms that are roughly uniformly distributed over many decades and reach extremely small values (Fig. 1). These eigenvalues quantify parameter space compression: A few stiff eigenvectors in each model point along directions where observables are sensitive to changes in parameters, whereas progressively sloppier directions make little difference. These sloppy parameter combinations cannot be inferred from collective data, and conversely, their exact values do not need to be known to quantitatively understand system behavior (*12*). Do physics models share this structure?

The diffusion equation is the canonical example of a continuum limit in physics. It governs behavior whenever small particles undergo

[1]Laboratory of Atomic and Solid State Physics, Cornell University, Ithaca, NY 14853, USA. [2]Lewis-Sigler Institute for Integrative Genomics, Princeton University, Princeton, NJ 08854, USA. [3]Department of Physics and Astronomy, Brigham Young University, Provo, UT 84602, USA.

*Corresponding author. E-mail: sethna@lassp.cornell.edu

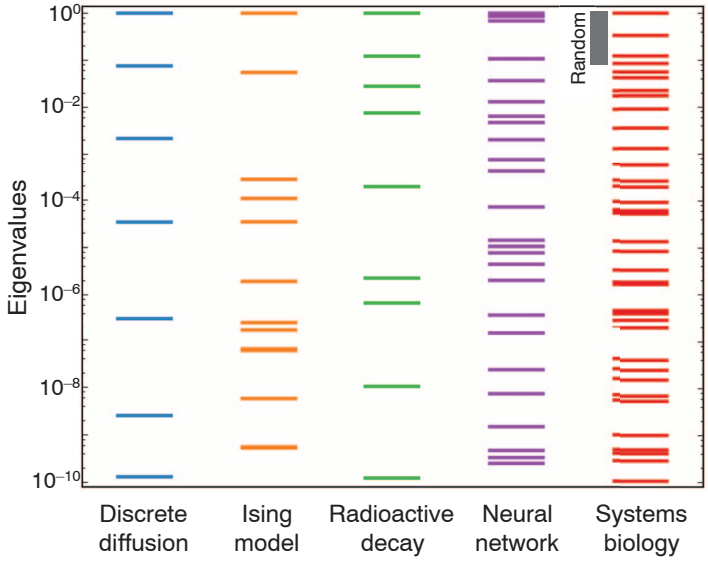

Fig. 1. Normalized eigenvalues of the FIM of various models. The diffusion and Ising models are explored here. A radioactive decay model and a neural network are taken from (*14*). The systems biology model is a differential equation model of a mitogen-activated protein kinase (MAPK) cascade taken from (*10*), and the adjoining band marked as "Random" shows a typical eigenvalue spread from a Wishart random matrix of the same size. (Additional examples are available in fig. S1.) In all models, the eigenvalues of the FIM are roughly geometrically distributed, with each successive direction substantially less important for system behavior (only the first 10 decades are shown). This means that inferring the parameter combination whose eigenvalue is smallest shown would require ~10^{10} times more data than would the stiffest parameter combination. Conversely, the least important parameter combination is $\sqrt{10^{10}}$ times less important for understanding system behavior.

stochastic motion. The complex microscopic collisions are described by a general linear dynamical equation for the particle density, $\rho(r, \tau)$:

$$\partial_\tau \rho(r,\tau) = R\rho - V\partial_x \rho + D\partial_x^2 \rho + \sum_{n=3}^{\infty} C_n \partial_x^n \rho \qquad (2)$$

Here, D is the diffusion constant, V is the net drift, R is the particle creation rate, coefficients C_n couple to higher-order gradient terms and scale as $C_n \propto \alpha^n$, where α is some microscopic length. As time τ proceeds, ρ smoothens over a length ~$\sqrt{D\tau}$. The contribution of higher-gradient terms thus scales as $C_n/(D\tau)^{n/2} \sim (D\tau/\alpha^2)^{-n/2}$ and can be dropped to yield the three-term diffusion equation as the emergent continuum limit. Microscopic parameters describing the particles and their environment enter into this continuum description only through their effects on D, V, and R. We considered a microscopic model of stochastic motion and particle creation on a discrete one-dimensional (1D) lattice of sites. Parameters θ^μ give the probabilities that a particle will be at site $j + \mu$ after one time step given a starting particle at site j, for $-N \le \mu \le N$ (Fig. 2, inset). At the initial time, all particles are at the origin, $\rho_0(j) = \delta_{j,0}$. The observables, $\vec{x} \equiv \rho_\tau(j)$, are the densities of particles at some later time τ.

After a single time step, the distribution of particles is given by $\rho_1(j) = \theta^j$. This distribution depends independently on all of its parameters; thus, the FIM is the identity, $g_{\mu\nu} = \delta_{\mu\nu}$ (*15*). Because each parameter is independently measurable, there is no parameter space compression. When particles take several time steps before their positions are observed, some parameter combinations affect observable behavior much more sensitively than do others: The nth FIM eigenvalue scales as $\lambda_n \sim \tau^2 (D\tau/a^2)^{-n-1/2}$ (Fig. 2) (*15*), where $a = N$ is the maximum hopping distance,

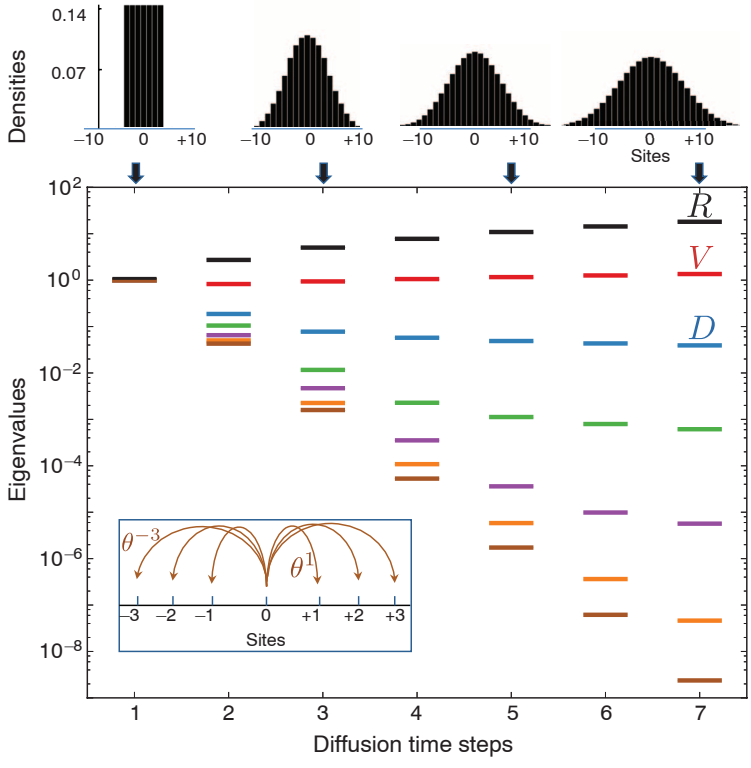

Fig. 2. FIM eigenvalues of a model of stochastic motion on a 1D lattice. The seven parameters describe probabilities of transitioning to nearby sites (bottom, inset). Observations are taken after a given number of time steps for the case in which all parameters take the value $\theta^\mu = 1/7$. The top row shows the resulting densities plotted at times $\tau = 1$, 3, 5, and 7. The bottom plot shows the eigenvalues of the FIM versus number of steps. After a single time step, the FIM is the identity, but as time progresses, the spectrum of the FIM spreads over many orders of magnitude. The first eigenvector measures deviations in the net particle creation rate R from 0, the second measures a net drift V in the density, and the third corresponds to parameter combinations that change the diffusion constant D. Further eigenvectors describe parameter combinations that do not affect these macroscopic parameters but instead measure the skew (green), kurtosis (purple), and higher moments of the resulting density (orange and brown).

our microscopic length scale. The information theory approach has automatically recapitulated the physics underlying the continuum limit; successive eigenvalues are separated by the square of the factor $\sqrt{D\tau/a^2}$ governing the strength of successive terms in the gradient expansion (Eq. 2). The three stiffest eigenvalues can be shown to correspond precisely to R, V,

and D; further eigenvectors control the skew, kurtosis, and higher moments of the final distribution of particles through coefficients C_n that do not appear in continuum descriptions (Fig. 2) (*15*). This gives an information theoretic explanation for the wide applicability of the diffusion equation and quantifies a widely held intuition: One cannot infer microscopic parameters such as the bond angle of a water molecule from a diffusion measurement. Conversely, microscopic details are unnecessary for understanding the long-scale behavior.

Continuum models such as the diffusion equation arise when fluctuations are large only on the microscale. These models are valid when the observables are slow and large when compared with the natural scale of fluctuations. RG methods clarify that system behavior can be quantitatively modeled even when fluctuations are large on all scales, such as near critical points and for quantum field theories. The Ising model is the prototypical system exhibiting these self-similar fluctuations. Near its critical point, the Ising model predicts fractal domains whose statistics are universal; it not only describes magnetic fluctuations in ferromagnets, but also the density fluctuations near a liquid-gas transition and composition fluctuations near a liquid-liquid miscibility transition (*19*, *20*). In the 2D square lattice Ising model, a "spin" at every site takes a value of $s_{i,j} = \pm 1$, and observables are spin configurations $\vec{x} = \{s_{i,j}\}$ or subsets $\vec{x}^n$, as defined below. Our generalized Ising model assigns to each spin configuration a probability given by its Boltzmann weight, $P_\theta(\vec{x}) = e^{-\mathcal{H}_\theta(\vec{x})}/Z$ and is parametrized through its Hamiltonian $\mathcal{H}_\theta(\vec{x}) = \theta^\mu \Phi_\mu(\vec{x})$. Parameters $\theta^{\alpha\beta}$ describe the coupling between spins and their neighbors at coordinates (α,β) away, so that $\Phi_{\alpha\beta}(\vec{x}) = \sum_{i,j} s_{i,j} s_{i+\alpha,j+\beta}$, whereas θ^0 is the external field multiplying $\Phi_0(\vec{x}) = \sum_{i,j} s_{i,j}$ (Fig. 3, inset) (*15*). The usual nearest-neighbor Ising model has $\theta^{01} = \theta^{10} = -1/T$, $\theta^0 = h$, and $\theta = 0$ otherwise. We examined our generalized model near the critical point $T = T_c$, $h = 0$ of the usual model.

At the microscopic level, observables are entire spin configurations, and the Ising FIM is a sum of two- and four-spin correlation functions that can be readily calculated by use of Monte Carlo techniques (*15*, *21*). The Ising model viewed at its microscopic scale has two-parameter combinations with large eigenvalues (Fig. 3, first column) (*15*). These two stiff eigenvectors control the so-called "relevant" variables of the RG, h and $t = (T - T_c)/T_c$, which affect long-distance behavior and have no analogy in the diffusion equation (*22*, *23*). The remaining eigenvalues all cluster around a scale given by the system size and do not yet show parameter space compression. Their distribution is reminiscent of the spectrum seen in the diffusion equation when viewed at its microscopic scale, at which parameters could be independently measured from particular observables. Their corresponding eigenvectors are nonstiff parameter combinations that only affect short-distance behavior ("irrelevant" RG variables). Nonetheless, the clustering of FIM eigenvalues (Fig. 3, first column) demonstrates that none of these parameter combinations are redundant for the description of microscopic data; a real "multiparameter" ferromagnet is not microscopically well-described by the two-parameter Ising model.

To understand how the Ising model provides a universal description for coarsened behavior, we restricted observables to spin configurations of a subset of lattice sites chosen via a checkerboard decimation procedure (Fig. 3, top row, insets). The FIM of Eq. 1 is now measured using as observables only those sites in a sublattice decimated by a factor 2^n, $\vec{x}^n = \{s_{i,j}\}_{\{i,j\} \in n}$. For example, one level of decimation corresponds to the black sites on the checkerboard, whereas after two steps, only sites $\{i,j\}$ with even i and j remain. The distribution is still drawn from the ensemble defined by the original Hamiltonian defined on the full lattice. The calculation was implemented by using Compatible Monte Carlo (*15*, *24*). The results from Monte Carlo are presented for a 64 × 64 lattice at its critical point in Fig. 3. From an information theory perspective, the results shown in Fig. 3 and analysis detailed in (*15*) demonstrate that relevant variables are exactly those for which spatial coarsening preserves measurement precision. Crucially, the other eigenvectors of the metric become progressively less important under coarsening, just as for diffusion. As coarsening proceeds, the FIM eigenvalues shrink according to the corresponding irrelevant RG exponent (Fig. 3) (*15*). The presence of just two stiff FIM eigenvalues provides an alternative explanation of why the two-parameter Ising model can capture the universal behavior of a wide variety of physical systems near their critical points.

We have seen that neither the diffusion model nor the Ising model are sloppy at their microscopic scales. It is only upon coarsening the observables—either by allowing several time steps to pass or by only observing a subset of lattice sites—that a typical sloppy spectrum of parameter combinations emerges. Correspondingly, multiparameter models such as in systems biology and other areas of science are sloppy only when fit to experiments that probe collective behavior; if experiments are designed to measure one parameter at a time, no model compression can be expected (*25*, *26*). In the models

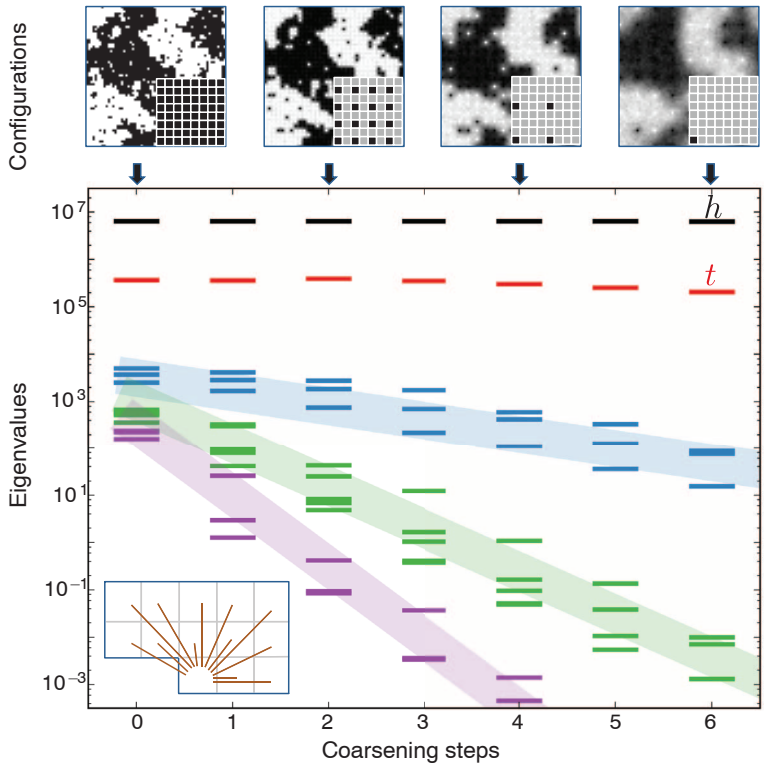

Fig. 3. FIM eigenvalues of an Ising model of ferromagnetism. Parameters describe nearest and nearby neighbor couplings (bottom, inset) and a magnetic field. Observables are spin configurations of all spins on a sublattice (dark sites in top, insets). (**Top**) One particular spin configuration generated by the model, suitably blurred for step > 0 to the average spin conditioned on the observed sublattice values. Some information about the configuration, such as the typical size of fluctuations, is preserved under this procedure, whereas other information such as the nearest-neighbor correlation amplitude is lost. The two largest eigenvalues, whose eigenvectors measure reduced temperature t and the applied field h do not decay substantially under coarsening. Further FIM eigenvalues shrink by a factor of $\sqrt{2}^{-2-2y_i}$, where y_i is the ith RG exponent (*15*). This shrinkage quantifies the information lost in each coarsening step.

examined here, there is a clear distinction between the short time or length scale of the microscopic theory and the long time or length scale of observables. As we show in (*15*), sloppiness in physics can be precisely traced to the ratio of these two scales—an important small variable. In the broad class of models in which such distinction of scales cannot be made, our explanation for sloppiness (*27*) is not yet unified with the RG and continuum methods of physics. Nonetheless, the striking similarity of their sloppy sensitivities lends perspective to the surprising power of mathematical modeling despite microscopic uncertainty.

References and Notes

1. E. P. Wigner, *Commun. Pure Appl. Math.* **13**, 1–14 (1960).
2. P. W. Anderson, *Science* **177**, 393–396 (1972).
3. U. Alon, *Nature* **446**, 497 (2007).
4. G. J. Stephens, B. Johnson-Kerner, W. Bialek, W. S. Ryu, *PLOS Comput. Biol.* **4**, e1000028 (2008).
5. G. J. Stephens, L. C. Osborne, W. Bialek, *Proc. Natl. Acad. Sci. U.S.A.* **108**, 15565–15571 (2011).
6. T. D. Sanger, *J. Neurosci.* **20**, 1066–1072 (2000).
7. F. Corson, E. D. Siggia, *Proc. Natl. Acad. Sci. U.S.A.* **109**, 5568–5575 (2012).
8. M. Schmidt, H. Lipson, *Science* **324**, 81–85 (2009).
9. T. Mora, W. Bialek, *J. Stat. Phys.* **144**, 268–302 (2011).
10. K. S. Brown *et al.*, *Phys. Biol.* **1**, 184–195 (2004).
11. R. N. Gutenkunst *et al.*, *PLOS Comput. Biol.* **3**, 1871–1878 (2007).
12. J. J. Waterfall *et al.*, *Phys. Rev. Lett.* **97**, 150601 (2006).
13. M. K. Transtrum, B. B. Machta, J. P. Sethna, *Phys. Rev. Lett.* **104**, 060201 (2010).
14. M. K. Transtrum, B. B. Machta, J. P. Sethna, *Phys. Rev. E Stat. Nonlin. Soft Matter Phys.* **83**, 036701 (2011).
15. Materials and methods are available as supplementary materials on *Science* Online.
16. S. Amari, H. Nagaoka, *Methods of Information Geometry* (American Mathematical Society, Providence, RI, 2000).
17. I. J. Myung, V. Balasubramanian, M. A. Pitt, *Proc. Natl. Acad. Sci. U.S.A.* **97**, 11170–11175 (2000).
18. V. Balasubramanian, *Neural Comput.* **9**, 349–368 (1997).
19. P. M. Chaikin, T. C. Lubensky, *Principles of Condensed Matter Physics* (Cambridge Univ. Press, Cambridge, 1995).
20. S. L. Veatch, O. Soubias, S. L. Keller, K. Gawrisch, *Proc. Natl. Acad. Sci. U.S.A.* **104**, 17650–17655 (2007).
21. G. E. Crooks, *Phys. Rev. Lett.* **99**, 100602 (2007).
22. J. Cardy, *Scaling and Renormalization in Statistical Physics* (Cambridge Univ. Press, Cambridge, 1996).
23. G. Ruppeiner, *Rev. Mod. Phys.* **67**, 605–659 (1995).
24. D. Ron, R. H. Swendsen, A. Brandt, *Phys. Rev. Lett.* **89**, 275701 (2002).
25. F. P. Casey *et al.*, *IET Syst. Biol.* **1**, 190–202 (2007).
26. J. F. Apgar, D. K. Witmer, F. M. White, B. Tidor, *Mol. Biosyst.* **6**, 1890–1900 (2010).
27. In (*13*, *14*), we used interpolation theorems and information geometry to show that multiparameter models fit to collective data have model manifolds that form hyper-ribbons in data space with geometrically spaced widths.

Acknowledgements: We thank S. Kuehn and S. Papanikolaou for helpful comments and discussions. This work was supported by NSF grants DMR 1005479 and DMR 1312160 and a Lewis-Sigler Fellowhip (B.B.M.). Raw data and analysis code are available on request from the authors or via the Internet: www.lassp.cornell.edu/sethna/Sloppy/EmergentParameterCompression.

Supplementary Materials

www.sciencemag.org/content/342/6158/604/suppl/DC1
Supplementary Text
Figs. S1 and S2
References (*28*–*42*)

4 April 2013; accepted 24 September 2013
10.1126/science.1238723

Deterministically Encoding Quantum Information Using 100-Photon Schrödinger Cat States

Brian Vlastakis,[1]* Gerhard Kirchmair,[1]† Zaki Leghtas,[1,2] Simon E. Nigg,[1]‡ Luigi Frunzio,[1] S. M. Girvin,[1] Mazyar Mirrahimi,[1,2] M. H. Devoret,[1] R. J. Schoelkopf[1]

In contrast to a single quantum bit, an oscillator can store multiple excitations and coherences provided one has the ability to generate and manipulate complex multiphoton states. We demonstrate multiphoton control by using a superconducting transmon qubit coupled to a waveguide cavity resonator with a highly ideal off-resonant coupling. This dispersive interaction is much greater than decoherence rates and higher-order nonlinearities to allow simultaneous manipulation of hundreds of photons. With a tool set of conditional qubit-photon logic, we mapped an arbitrary qubit state to a superposition of coherent states, known as a "cat state." We created cat states as large as 111 photons and extended this protocol to create superpositions of up to four coherent states. This control creates a powerful interface between discrete and continuous variable quantum computation and could enable applications in metrology and quantum information processing.

Cavity quantum electrodynamics is a testbed system for quantum optics, allowing the observation of strong interactions between photons and (artificial) atoms (*1*–*3*). Techniques using these systems allow the production of nonclassical states of light, which have important uses for quantum communication, quantum computation, and investigations of fundamental quantum theory. For superconducting quantum circuits, cavity resonators have proven a valuable resource serving several roles: a quantum bus to generate entanglement between qubits (*4*), a quantum nondemolition probe allowing efficient quantum measurements (*5*, *6*), a generator of single microwave photons (*7*, *8*), and a quantum memory to store and shuttle information (*9*, *10*). With its large Hilbert space, a cavity resonator also has the potential to store multiple quantum bits or redundantly encode information as necessary for quantum error correction. With the proper controls, a single cavity could be made equivalent to a multiqubit register, allowing for simplifications of hardware design (*11*, *12*). Although there have been some investigations of complex, multiphoton superpositions in superconducting cavity resonators, most techniques developed so far require fast qubit frequency tunability and are based on controlling individual photons one by one (*13*, *14*). These implementations become increasingly burdensome for complex states or large photon numbers, making it desirable to develop a more natural method for controlling the large cavity Hilbert space.

We demonstrated a set of multiphoton operations by using a fixed-frequency superconducting transmon qubit coupled to a waveguide cavity resonator. We realized a highly ideal strong-dispersive coupling, where the strengths of the off-resonant qubit-cavity interactions were several orders of magnitude greater than the cavity decay rate and higher-order nonlinearities. This created a set of qubit-cavity entangling operations, allowing for control over the large cavity phase space. We implemented two of these operations: the qubit-state conditional cavity phase shift (*15*) and the photon-number conditional qubit rotation (*14*, *16*). We combined these with unconditional qubit and cavity operations to perform direct measurements of the cavity Wigner function (*17*) and to efficiently generate large superposition states. By using these tools, we realized a recently proposed protocol (*18*) to deterministically encode quantum information in a cat state by creating an arbitrary superposition of quasi-orthogonal coherent states conditioned on an initial qubit state. We concatenated these entangling operations to encode quantum information into multiple phases of the cavity state, thereby creating multicomponent cat states and producing example states

[1]Department of Physics and Department of Applied Physics, Yale University, New Haven, CT 06511, USA. [2]Inria Paris-Rocquencourt, 78153 Le Chesnay Cedex, France.

*Corresponding author. E-mail: brian.vlastakis@yale.edu
†Present address: Institut für Quantenoptik und Quanteninformation, Österreichische Akademie der Wissenschaften, Otto-Hittmair-Platz 1, A-6020 Innsbruck, Austria, and Institut für Experimentalphysik, Universität Innsbruck, Technikerstrasse 25, A-6020 Innsbruck, Austria.
‡Present address: Department of Physics, University of Basel, CH-4056 Basel, Switzerland.

EXTENDED PDF SPONSORED
BY BIO-TECHNE.COM
bio-techne
LIFE SCIENCE BRANDS
R&D systems NOVUS BIOLOGICALS TOCRIS
LEARN MORE
http://bio-techne.com/launch/?utm_source=Science.com
&utm_medium=PDF%20banner&utm_campaign=Launchv2

Parameter Space Compression Underlies Emergent Theories and Predictive Models

Benjamin B. Machta *et al.*

Science **342**, 604 (2013);
DOI: 10.1126/science.1238723

This copy is for your personal, non-commercial use only.

If you wish to distribute this article to others, you can order high-quality copies for your colleagues, clients, or customers by clicking here.

Permission to republish or repurpose articles or portions of articles can be obtained by following the guidelines here.

The following resources related to this article are available online at www.sciencemag.org (this information is current as of January 1, 2015):

A correction has been published for this article at:
http://www.sciencemag.org/content/342/6161/931.2.full.html

Updated information and services, including high-resolution figures, can be found in the online version of this article at:
http://www.sciencemag.org/content/342/6158/604.full.html

Supporting Online Material can be found at:
http://www.sciencemag.org/content/suppl/2013/10/30/342.6158.604.DC1.html

A list of selected additional articles on the Science Web sites **related to this article** can be found at:
http://www.sciencemag.org/content/342/6158/604.full.html#related

This article **cites 33 articles**, 8 of which can be accessed free:
http://www.sciencemag.org/content/342/6158/604.full.html#ref-list-1

This article has been **cited by** 2 articles hosted by HighWire Press; see:
http://www.sciencemag.org/content/342/6158/604.full.html#related-urls

This article appears in the following **subject collections:**
Physics
http://www.sciencemag.org/cgi/collection/physics

Downloaded from www.sciencemag.org on January 1, 2015

Science (print ISSN 0036-8075; online ISSN 1095-9203) is published weekly, except the last week in December, by the American Association for the Advancement of Science, 1200 New York Avenue NW, Washington, DC 20005. Copyright 2013 by the American Association for the Advancement of Science; all rights reserved. The title *Science* is a registered trademark of AAAS.